Available online at www.sciencedirect.com
ScienceDirect
Journal of Crystal Growth 310 (2008) 2832–2841
JOURNAL OF CRYSTAL GROWTH
www.elsevier.com/locate/jcrysgro

Synthesis of calcium carbonate polymorphs in the presence of polyacrylic acid

S. Ouhenia[a,b,*], D. Chateigner[b], M.A. Belkhir[a], E. Guilmeau[b], C. Krauss[b]

[a]*Laboratoire de Physique, Faculté des Sciences et Sciences de l'ingénieur, Béjaïa 06200, Algeria*
[b]*Laboratoire CRISMAT-ENSICAEN (CNRS UMR 6508), Université de Caen Basse-Normandie, 6 bd M. Juin 14050, Caen, France*

Received 1 October 2007; received in revised form 18 January 2008; accepted 8 February 2008
Communicated by K. Sato
Available online 16 February 2008

Abstract

Calcium carbonate precipitates are prepared from a solution of $CaCl_2$ and K_2CO_3 in the presence of polyacrilic acid. The effect of polyacrilic acid incorporation in the [25–80 °C] temperature range on crystal morphologies and $CaCO_3$ precipitated polymorph concentrations are investigated using scanning electron microscopy and X-ray diffraction quantitative microstructural and phase analysis. Large changes in morphology and phase proportions are observed in the presence of polyacrylic acid, which strongly depend on the solution temperature. While crystallization of vaterite is favoured in the presence of polyacrilic acid up to 50 °C, it is largely destabilized at higher temperatures. Our process also enables the elaboration of particles in the range 10–20 nm.

PACS: 61.10.Ng; 81.10.Dn; 61.46.Hk

Keywords: A1. Biomineralization; A1. Hybrid materials; B1. Calcium carbonate

1. Introduction

It is well known that biomineralization is an elaborated process that produces biominerals with complex morphologies as well as superior mechanical properties [1–4]. The complete understanding of biomineral development processes is still a subject of debates and is strongly motivated by their potential utility in industrial and biomedical applications [5]. Calcium carbonate polymorphs are some of the most abundant mineral phases incorporating biomineralized tissues, e.g. in mollusk shells where calcite and aragonite often coexist in adjacent shell layers [6–8]. Aragonitic biominerals like nacre layers from *Pinctada magaritiferra* are also seen as ideal biomedical implants or, thanks to their high aspect ratio, aragonite crystals can be used as reinforcements in composite materials [9]. $CaCO_3$ has three anhydrous crystalline polymorphs: calcite, aragonite and vaterite. Calcite is thermodynamically the most stable phase, whereas vaterite is the least stable one and transforms into one of the other two forms. Vaterite particles do not show well-defined morphologies, and usually aggregate into spherical particles [10]. In the recent years, inspired by the effect of additives, vaterite appeared in various morphologies [10–13]. Among the possible additives, surfactants, with charged head groups, can combine with some ions or absorb on some faces of crystals. They turned out to be very effective in controlling the morphology of inorganic materials [14].

Numerous studies have been carried out to understand the influence of organic molecules on the $CaCO_3$ particle growth. Many studies showed a correlation between the calcium carbonate growth modifications and the structure of the additive organic molecules [15–19]. However, difficulties in understanding their respective roles arise from the complexity of the study of such mechanisms in the solid–liquid system [20] and the large ability of the CO_3^{2-} anions to form different supramolecule structures.

*Corresponding author at: Laboratoire CRISMAT-ENSICAEN (CNRS UMR 6508), Université de Caen Basse-Normandie, 6 bd M. Juin 14050, Caen, France.
E-mail address: salim.ouhenia@ensicaen.fr (S. Ouhenia).

0022-0248/$ - see front matter © 2008 Elsevier B.V. All rights reserved.
doi:10.1016/j.jcrysgro.2008.02.006

Recently some studies [21–23] showed that surfactants can influence the $CaCO_3$ nucleation, crystal growth and grain shapes, and, consequently, control the formation of crystal phases that are not usually stabilized under natural environments. Such surfactants have been used as micro-reactors for the preparation of specific morphologies, sizes, or crystal structures of organic materials [24,25].

Aragonite is metastable at room temperature and transforms to calcite in a natural environment. Many attempts have been made to mimic the biological synthesis of aragonite using different organic substrates and additives; for example, aragonite thin films formed on polyvinyl alcohol (PVA) matrices in the presence of polyacrilic acid (PAA) [26], aragonite whiskers using cetyltrimethylammonium bromide (CTAB) [26] and pure aragonite prepared in the presence of sodium benesulfonate (SDBS) [27].

In this work, we study the crystallization of $CaCO_3$ particles from aqueous solutions in the presence of PAA. The PAA's effects on the crystals' morphology, crystals' mean sizes and polymorphs' volume contents at temperatures varying from 25 to 80 °C are examined using scanning electron microscopy (SEM) and X-ray quantitative phase analysis.

2. Experimental procedure

2.1. Materials

PAA ([-$CH_2CH(CO_2H)$-]*n*) from Acros Organics chemical company (USA) with an average molecular weight of ca. 240,000, calcium chloride ($CaCl_2$) and potassium carbonate (K_2CO_3) from Prolabo were used as reactants. All chemicals were of analytical grade and used without further purification. Doubly deionized water was used to prepare 0.1 M $CaCl_2$ and 0.1 M K_2CO_3 aqueous solutions. The solution of $CaCl_2$ is divided into two parts, one of them is mixed to PAA. The proportion is 0.5 mg of PAA in 5 ml of $CaCl_2$. The two solutions are mixed at different temperatures: 20, 50, and 80 °C. The solid precipitates, obtained immediately after mixing the two solutions, were collected using filtration through a cellulose membrane filter, and rinsed three times with doubly dionized water. Finally, the $CaCO_3$ precipitates were dried under vacuum at 100 °C for 1 h, resulting in finely grained powders.

2.2. Characterization

All the samples were examined using SEM (Zeiss electron microscope) with an accelerating voltage of 15 kV. X-ray diffraction (XRD) patterns were collected on a Phillips X'PERT powder diffractometer using the CuK_α radiation using a scan step of 0.017° 2θ. The volumic ratios of calcite (space group: $R\bar{3}c$), vaterite (S.G: $P6_3/mmc$) and aragonite (S.G: Pmcn) phases of the samples were calculated using the quantitative phase analysis based on the Rietveld method [28,29], implemented in the MAUD software [30]. The crystallite mean sizes were refined using an isotropic model without microstrain, deconvoluted from the instrument calibration curve. All the three phases were declared in the diagrams and the phase content parameters released for two of them, constraining the sum to 100% volume. During the Rietveld refinement, cell parameters were also released to get the best reliability factors. No preferred orientation was detected in the diagrams. In the diffraction diagrams no signal from the organic PAA matrix is expected due to its relatively weak contrast compared to mineral phases, and its strongly amorphous character.

3. Results and discussion

3.1. Effect of PAA on $CaCO_3$ polymorphs at 25 °C

Fig. 1 shows SEM micrographs of $CaCO_3$ particles obtained at 25 °C without PAA. A mixture of interpenetrated rhombic- (Fig. 1a) and spherical-like particles is observed. The average edge and diameter of the interpenetrated rhombic (calcite) and spherical (vaterite) particles are 3 and 4 μm, respectively. The refinement converges to a reasonably good solution with low reliability factors (Table 1) and a pretty flat difference curve (Fig. 8a). These results coincide with the observed crystallite shapes corresponding to regular crystallization for such temperatures, with spherical vaterite and calcite rhomboids. The Rietveld quantitative phase analysis shows that the volume fraction of calcite is 71(1)% and hence 29(1)% of vaterite with no aragonite (Table 1). The average size of the crystallites is 870(5) Å for calcite and 161(3) Å for vaterite. The relatively low size of the vaterite coherent domains explains the peak broadening of this phase visible in the respective diagram. The observed vaterite spherical particles, of typically several micrometers in diameter, exhibit a very porous substructure using a larger magnification (Fig. 1b). This original substructure accommodates a quite perfect sphere with acicular crystallites disposed radially, and having typically a mean diameter of 50–100 Å and a total length around 500 Å. This explains a mean coherent size around 161 Å determined from the XRD patterns, and consequently points out that these acicular crystals are composed of only one coherent domain on an average. Such vaterite particles would probably exhibit very high specific surfaces. The calcite crystals exhibit step-like edges due to the interpenetration of the constituting rhombs (Fig. 1c). The XRD mean size is also observed to be smaller than the calcite crystals seen by SEM, and accounts for crystal imperfections visible as straight lines on such images.

In the presence of PAA at 25 °C (Fig. 2a), one can observe that the previous calcite and vaterite mixture has been modified. On one hand, the calcite rhombs, although exhibiting less interpenetration, show less regular faces with more steps and porosities. On the other hand, the vaterite particles agglomerate in overall raspberry shapes

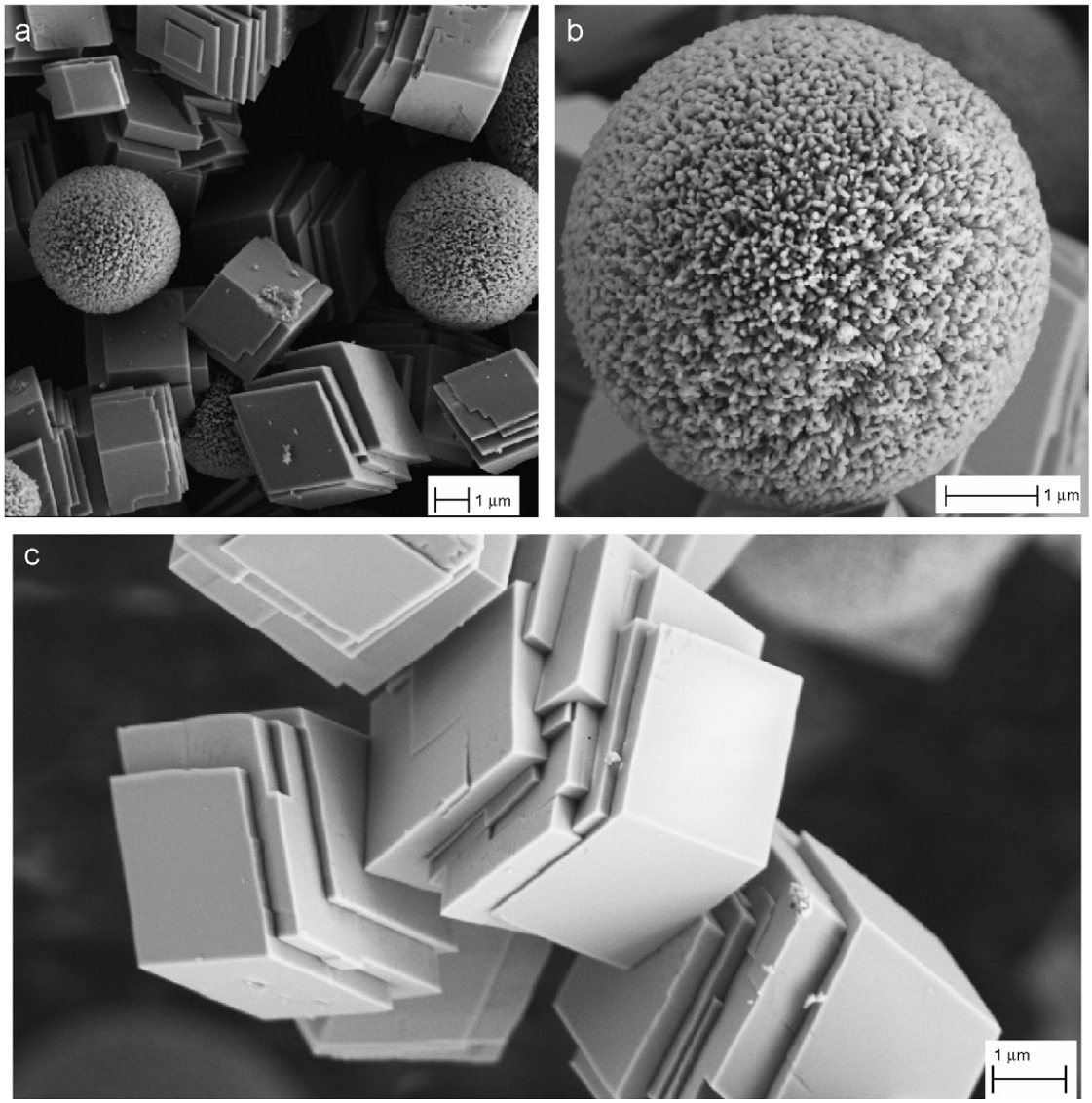

Fig. 1. SEM backscattered images of $CaCO_3$ particles synthesized at 25 °C without PAA incorporation. (a) Low-magnification image, and zoom on (b) vaterite spheres and (c) calcite interpenetrated rhombs.

of about 15 μm in widths, each initially individual vaterite sphere being deformed (Fig. 2b). The calcite particles have grown to around 10-μm edged rhombs (Fig. 2c). The difference in particle shape is clearly due to the presence of PAA in the solution. On PAA addition at this temperature, calcite is destabilized in volume but results in 10 times larger rhombs on an average with less acute edges and faces, and correlatively vaterite growth is favoured up to 50% in volume, but with deformed spheres that glue together in raspberry-like conglomerates. The refinement converges to a reasonably good solution with low reliability factor, and a flat difference curve has been obtained (Fig. 8b). The refinement provides crystallite sizes of 2960(99) and 203(3) Å for calcite and vaterite, respectively. This indicates clearly that the presence of PAA in soft enough conditions (at low enough temperatures) helps both calcite and vaterite growing, with an overall volumic balance in favour of vaterite. This change in crystal habits is accompanied by a reduction of cell parameters for calcite (with a 0.075% volume decrease, Table 1) as a result of the PAA–calcite interaction, while vaterite unit cell increases in volume in 0.23%.

3.2. *Effect of PAA on $CaCO_3$ polymorphs at 50 °C*

Fig. 3a shows the morphology of $CaCO_3$ particles produced at 50 °C without PAA. At this temperature, a mixture of three types of particle shapes is observed: calcite rhombs exhibiting an average edge size of nearly 5 μm (Fig. 3b), raspberry agglomerates of vaterite with an average diameter of 10 μm (Fig. 3c) and cauliflower-shaped particles of aragonite with an average diameter around 20 μm (Fig. 3d). The rhombic calcite particles exhibit more regular shapes than at 25 °C without PAA, and in particular interpenetration of rhombs is no longer visible. However, calcite crystals show starting erosion from the

Table 1
Refined parameters obtained by Rietveld refinement and quantitative phase analysis using MAUD

Phase	a (Å)	b (Å)	c (Å)	Vol. fraction	Crystallite mean isotropic size (Å)	Rb (%), Rw (%), R_{exp} (%), X^2
25 °C, without PAA.25 °C, without PAA.						
Calcite	4.9948(2)		17.0814(8)	0.71(1)	870(5)	6.53, 8.18, 5.34, 1.53
Vaterite	4.1236(9)		8.476(4)	0.29(1)	161(3)	
25 °C, with PAA.						
Calcite	4.9934(1)		17.0780(7)	0.495(6)	2960(99)	9.79, 12.34, 4.85, 6.60
Vaterite	4.1280(4)		8.478(2)	0.505(6)	203(3)	
50 °C, without PAA.						
Calcite	4.9962(2)		17.086(1)	0.47(3)	999(18)	6.81, 8.40, 5.33, 2.46
Vaterite	4.1232(5)		8.484(2)	0.46(3)	216(5)	
Aragonite	4.963(2)	7.953(4)	5.758(2)	0.07(6)	433(55)	
50 °C, with PAA.						
Calcite	4.9909(2)		17.067(1)	0.102(2)	3900(350)	9.84, 12.24, 4.55, 7.18
Vaterite	4.1281(2)		8.474(1)	0.79(1)	438(6)	
Aragonite	4.963(1)	7.953(3)	5.758(2)	0.108(3)	626(27)	
80 °C, without PAA.						
Calcite	4.9898(3)		17.062(1)	0.069(1)	1975(269)	5.05, 6.86, 4.74, 2.28
Vaterite	4.1273(3)		8.4653(6)	0.127(6)	581(56)	
Aragonite	4.9601(1)	7.9721(2)	5.7496(2)	0.80(7)	443(4)	
80 °C, with PAA.						
Calcite	4.9876(3)		17.048(1)	0.087(4)	1569(91)	7.25, 9.17, 4.84, 3.57
Vaterite	4.132(2)		8.46(2)	0.015(3)	477(97)	
Aragonite	4.9589(1)	7.9705(2)	5.7446(1)	0.89(1)	472(2)	

Parentheses indicate the estimated standard deviation on the last digit(s) of the parameters.

rhombs' face centres inward, acting as small slabs removal. This face centred erosion (FCE) could come from a larger solubility due to temperature, eventually helped by the presence of specific crystalline defects in the centres of the rhomb faces. X-ray quantitative phase analysis (Fig. 8c) indicates 47(3)% of calcite, 46(3)% of vaterite and 7(3)% of aragonite, which is coherent with the visual proportions of SEM images, pointing out that calcite transformation is operated for $\frac{2}{3}$ and $\frac{1}{3}$ approximately into vaterite and aragonite at this temperature. The crystallite sizes are 999(18) Å for calcite, 216(5) Å for vaterite and 433(55) Å for aragonite. The increase in mean crystallite sizes of calcite and vaterite (around 15% and 34%, respectively) is neatly in favour of vaterite formation compared to the sample elaborated at 25 °C without PAA. This is linked to the progressive equilibrium shift towards vaterite formation at a larger temperature.

At this temperature of 50 °C, PAA incorporation transforms the cauliflower-shaped particles of aragonite into dendritic particles with an average length of 10 μm (Fig. 4a) and the raspberry-like vaterite opens into flower-like conglomerates (Fig. 4b) with an average diameter of 5 μm. Such flower-like configuration has already been observed [31] on an eggshell membrane. A small amount of rhombic calcite is observed (Fig. 4c), on which we see again the porosity observed at 25 °C in the presence of PAA, together with the FCE effect. This means that FCE is not influenced by PAA but temperature, the former influencing more the internal crystallization of the polymorphs. Quantitative phase analysis (Fig. 8d) shows a strong decrease of the volume fraction of calcite in favour of vaterite, and to a lesser extent of aragonite. We can also see a significant increase of the crystallites size of calcite (3900(350) Å) and vaterite (438(6) Å) which confirms the beneficial effect of PAA incorporation for crystal growing, as already observed at 25 °C. A decrease in calcite unit-cell volume of 0.32%, while a 0.1% increase of the unit-cell volume of vaterite are observed, and aragonite unit-cell remains unaffected in our resolution limit. The effect of PAA inclusion on vaterite growth and calcite destabilization is then observed among the selected $CaCO_3$ polymorphs. Furthermore, PAA inclusion in vaterite is anisotropic, operating a tensile effect on the cell parameter, while a compression on c. This is coherent with carbonate groups parallel to the c-axis in vaterite [32], and PAA bounding to oxygen planes of the C–O groups along the a-axis. Similar unit-cells distortion has already been observed in biogenic aragonite crystals, but to a lesser extent [33], using high-resolution diffraction. They have been attributed to aplanarity of the carbonate groups, resulting from interaction between organic macromolecules and growing crystallites during biomineralization. In our case such an interaction is also revealed between PAA and the inorganic phases, and is visible for the vaterite allotropic form of calcium carbonate.

3.3. Effect of PAA on $CaCO_3$ polymorphs at 80 °C

Fig. 5 shows the morphology of $CaCO_3$ particles at 80 °C without PAA. Aragonite cauliflowers continued to grow

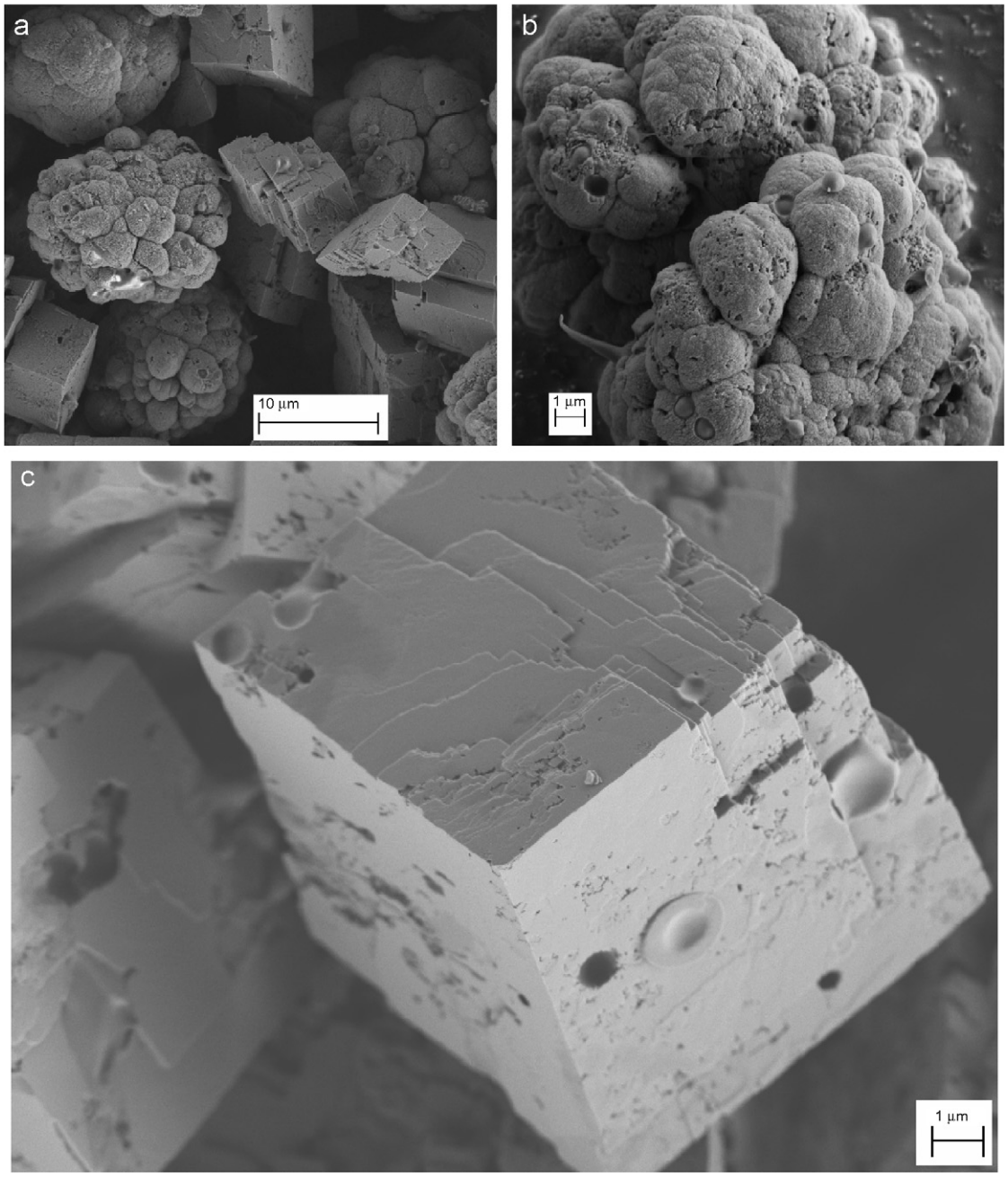

Fig. 2. SEM backscattered images of $CaCO_3$ particles synthesized at 25 °C in the presence of PAA. (a) Low-magnification image, and zoom on (b) vaterite raspberries and (c) calcite regular but porous rhombs.

into acicular crystals at this temperature (Fig. 5a), with an average length of typically 5–10 µm, and a smaller mean dimension less than 1 µm. A small amount of calcite particles with a perfect 2–4 µm-edge rhombohedral shape and a small amount of vaterite exhibiting a sponge-like shape (Fig. 5b) are also observed. The volume fractions are (Fig. 8e) 6.9(1)%, 12.7(6)%, and 80(7)% for calcite, vaterite, and aragonite, respectively. As usual at larger temperatures, aragonite formation is favoured at the expense of the two other phases, linked to the increase in calcium coordination at larger temperatures. The cell parameters of the aragonite are the closest to the bulk parameter values, as expected for its better crystallization at this temperature.

With PAA (Fig. 6), aragonite needles are cut into smaller pieces of around 4 µm in length and small amounts of calcite and vaterite are observed, with a global further increase of aragonite content to 89(1)% in volume. The crystallite sizes are lowered with PAA incorporation for calcite and vaterite, correlatively, with their destabilization at this temperature (this size decreasing is already observed without PAA compared to the 50 °C sample). This destabilization is also underlined by the unit-cell decrease of calcite, whereas the unit cell volume of the remaining

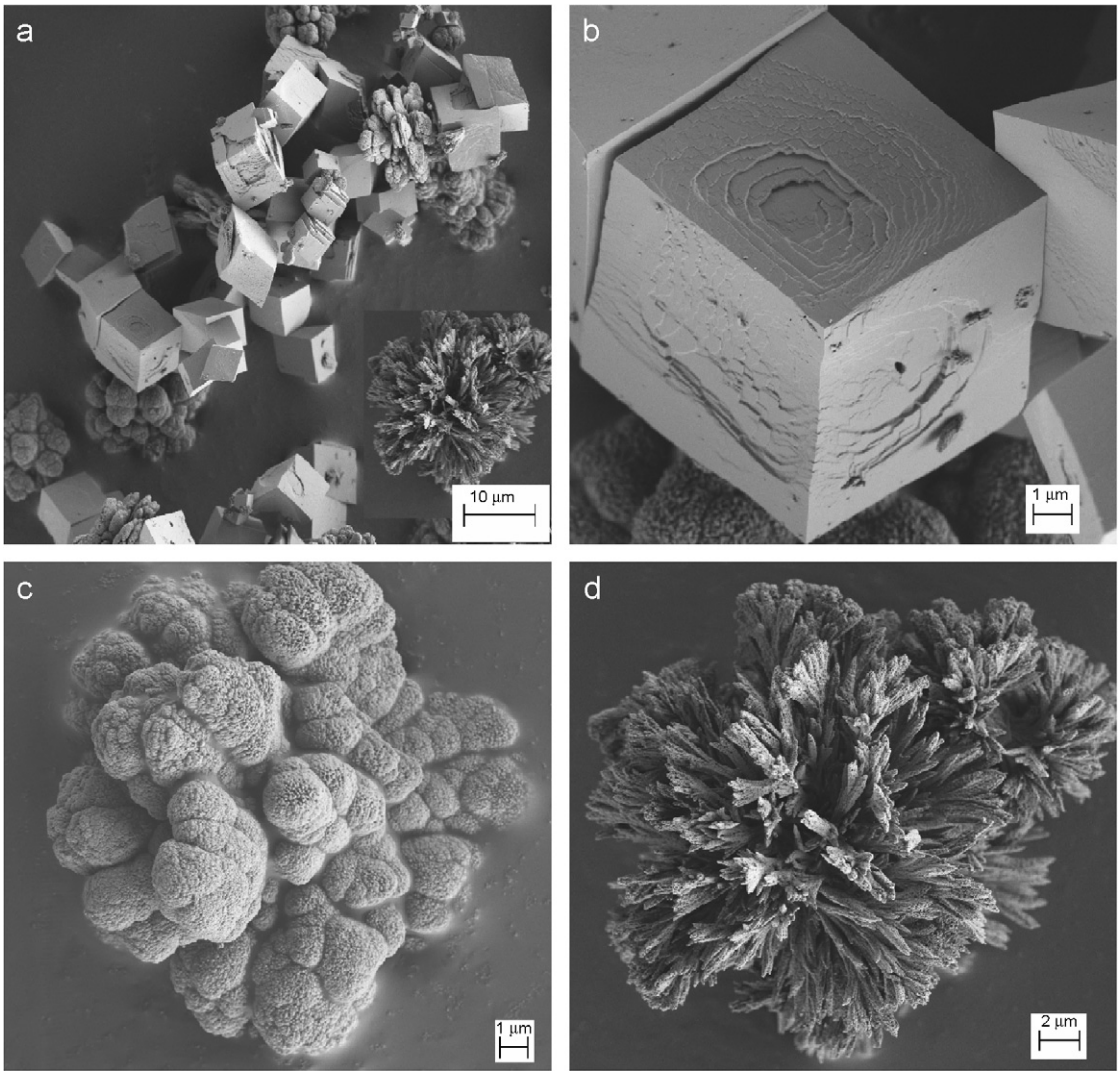

Fig. 3. SEM backscattered images of $CaCO_3$ particles synthesized at 50 °C without PAA incorporation. (a) Low-magnification image and zoom on (b) calcite regular rhombs with FCE, (c) vaterite raspberries, and (d) aragonite cauliflowers.

vaterite still increases in the presence of PAA, anisotropically like at 50 °C.

3.4. Effect of PAA on crystallization behaviours and morphologies of $CaCO_3$ crystals

Full mechanisms of how PAA controls $CaCO_3$ crystal growth for the three polymorphs are still matter of conjectures. From the work of Pan et al. [34] we chose to use low concentrations of PAA in the solution in order to ascertain its complete dissociation, and liberate H^+ protons in the solution following the reaction:

$$PAA \leftrightarrow PAA(COO) + H^+ \quad (1)$$

In the resulting acidic conditions, $CaCl_2$ solubility is increased, giving rise to more Ca^{2+} ions in the solution that serve the formation of PAA-Ca^+ polyelectrolyte complexes in the solution via the following reaction:

$$PAA(COO^-) + Ca^{2+} \leftrightarrow PAA(COO)Ca^+ \quad (2)$$

It is well known that aragonite needle-like crystals predominately grow in the direction of their *c*-axes upon crystallization from supersaturated solution [32,35]. The complexes resulting from reaction (2) are rapidly formed, and it seems reasonable to hypothesize that this reaction takes place wherever highly energetic sites are present. In the case of aragonite such sites are found preferentially on faces parallel to the *c*-axes, i.e. where oxygen atoms from carbonate groups are most located. Resultantly, complexes' adsorption on these faces block further growth perpendicularly to the needle axes and prevent aragonite transformation into calcite, giving rise to an increase in aragonite content. Under temperature conditions for which aragonite acicular crystals nucleate, i.e. from around 40 °C on, crystal shapes are kept as needle-like [36], either as isolated needles (Fig. 6) or as dendrite-like aggregates (Fig. 4a), depending on the temperature of the solution, with larger affinity to grow as single needles for larger temperatures.

A similar interpretation can be carried out for vaterite, though the crystal shapes differ. In vaterite, oxygen sites

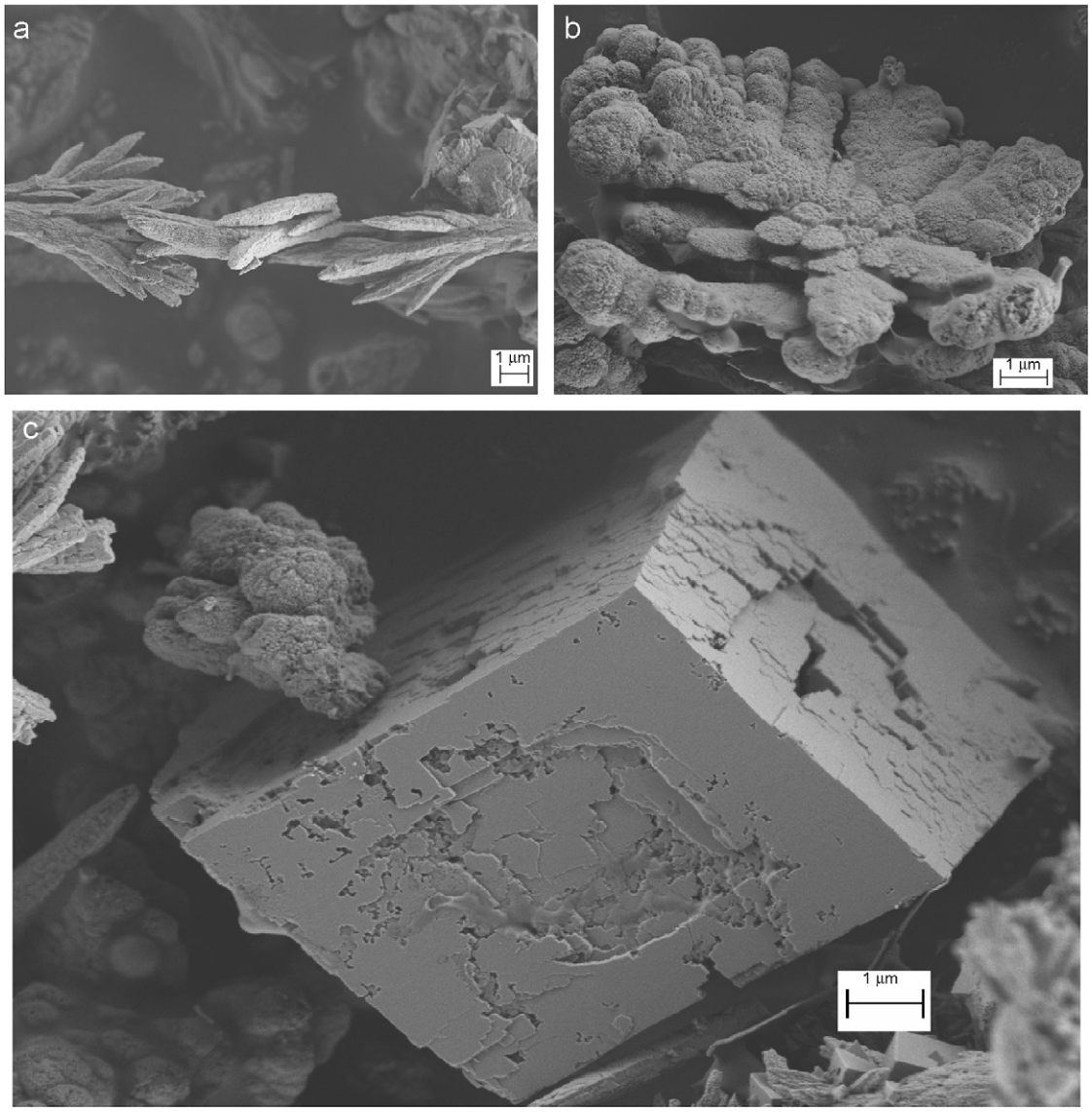

Fig. 4. SEM backscattered images of $CaCO_3$ particles synthesized at 50 °C in the presence of PAA. Zoom on (a) aragonite dendrites, (b) vaterite flowers, and (c) calcite porous rhombs with FCE.

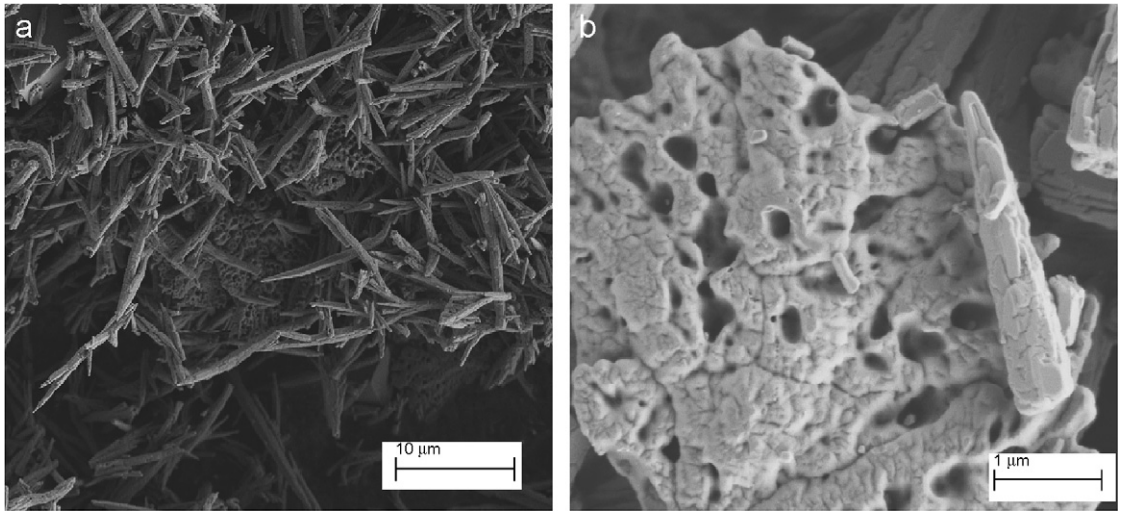

Fig. 5. SEM backscattered images of $CaCO_3$ particles synthesized at 80 °C without PAA incorporation: (a) acicular aragonite particles with some calcite rhombs, and (b) vaterite sponges.

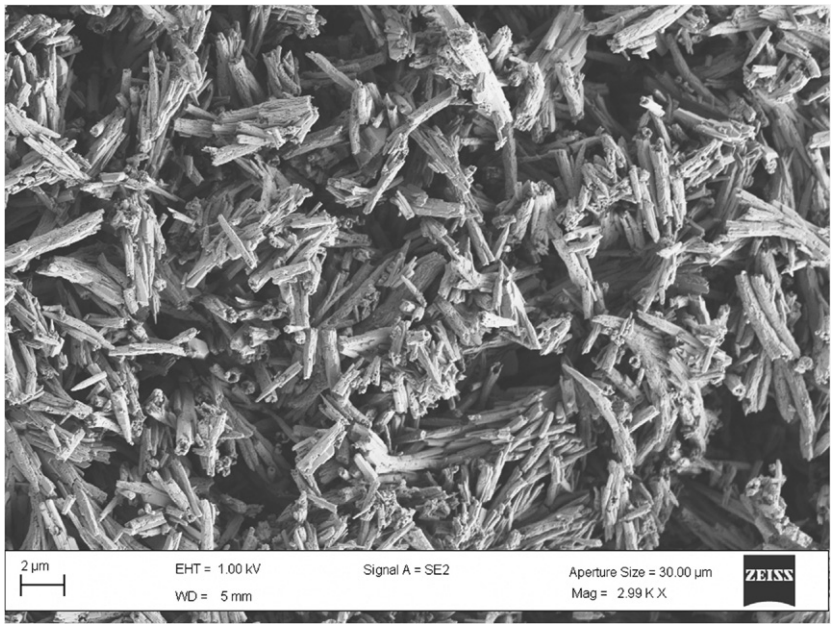

Fig. 6. SEM backscattered images of $CaCO_3$ particles synthesized at 80 °C in the presence of PAA. Only aragonite needles are observed.

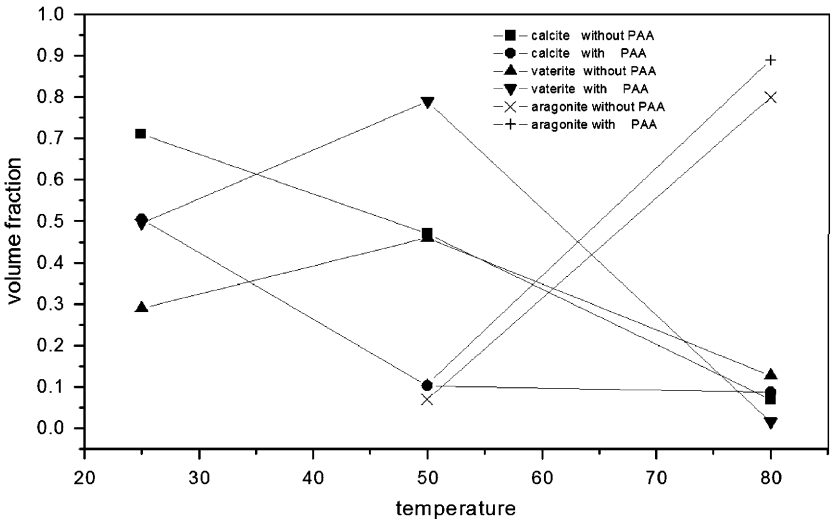

Fig. 7. Volume fraction of $CaCO_3$ polymorphs in the presence or not of PAA versus temperature.

also occur along faces parallel to the *c*-axes, and this phase is by far the less thermodynamically stable over the three polymorphs. It is then coherent in the energetic considerations of the previous paragraph that PAA complexes adsorb preferentially on vaterite as far as it is nucleated for a given temperature. At low temperatures (25 °C), the porosities of the sphere-like vaterite particles (Fig. 1b) are filled by further vaterite growing under PAA complexes, giving rise to the raspberry shapes by aggregation of several spheres. At intermediate temperatures (50 °C) for which vaterite is favored, the initial rounded conglomerates (without PAA, Fig. 3c) develop further under PAA influence. At larger temperatures vaterite is destabilized.

When PAA is used, the roughness of the calcite faces increases. This can be explained by the fact that the formation of the polyelectrolyte complexes decreases the Ca^{+2}-free ions in the solution. Pan et al. [37] observed a similar erosion behaviour of calcite rhombs when only PAA is used, giving rise to rough rhombs with uneven surfaces due to strong interactions between PAA carboxyl acid groups and $CaCO_3$. Their experiments resulted in similar mean diameters of the calcite grains, even if the latter were transformed into hollow spheres with addition of surfactants. In our conditions, calcite dissolves under acidic conditions, at the benefit of the complex and aragonite and vaterite formations, depending on the temperature.

3.5. Volume fractions variation in the presence or not of PAA

The volume fraction of the different polymorphs versus temperature, in the presence or not of PAA, is shown in Fig. 7. Without PAA, the volume fraction of calcite decreases linearly with temperature, varying from 71% at 25 °C to practically less than 10% at 80 °C. The presence of PAA decreases even more the volume fraction of this most stable phase from less than 50% at 25 °C to 10% at 50 °C. Concerning vaterite, one can observe a strong increase of this phase fraction from 25 to 50 °C, but an even more

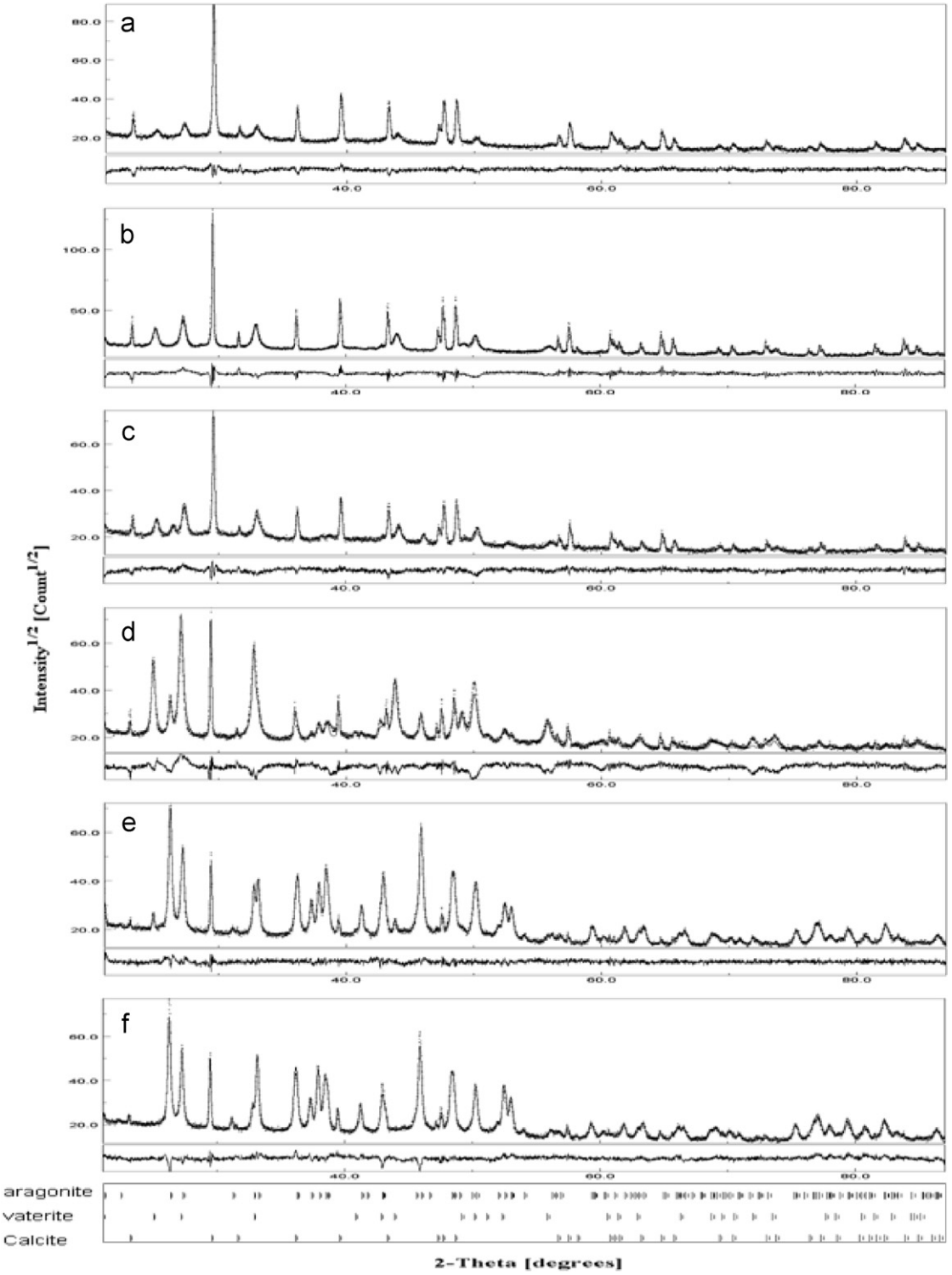

Fig. 8. Calculated (lines), observed (dots), and difference curves after the last cycle of Rietveld refinement for quantitative phase analysis: (a) 25 °C without PAA; (b) 25 °C with PAA; (c) 50 °C without PAA; (d) 50 °C with PAA; (e) 80 °C without PAA; and (f) 80 °C with PAA.

abrupt decrease from 50 to 80 °C than for calcite, a decrease amplified by the presence of PAA. Vaterite is then favoured by PAA incorporation at middle temperatures, but this PAA effect is reverse at temperatures larger than typically 70 °C. The aragonite phase also benefits from PAA incorporation, as soon as the phase can form in large enough volumes to be detected (50 °C), and the effect of PAA accentuates at the largest temperatures probed (Fig. 8).

4. Conclusion

The PAA and the temperature have been used as templates to induce $CaCO_3$ crystal growth. Various morphologies of $CaCO_3$ particles, such as rhombohedral, spherical, cauliflower, needles- and sponge-like, have been elaborated in the 25–80 °C temperature range by a simple method, which provides an easy route to the monitoring of $CaCO_3$ morphologies. Our results indicate that PAA can shift the chemical equilibrium between the allotropic forms of $CaCO_3$, thereby increasing vaterite and aragonite fractions depending on the temperature used. This result could be used in places where calcite is undesired. PAA can also control crystal sizes, quality, and shapes, via processes that modify unit-cell parameters of the respective phases. There is then a strong interaction of PAA with $CaCO_3$ that could help understanding the growth of natural biominerals.

References

[1] J.D. Currey, J.D. Talor, J. Zool. London 173 (1974) 395.
[2] J.D. Currey, A.J. Kohn, J. Mater. Sci. 11 (1976) 1615.
[3] J.D. Currey, J. Zool. London 180 (1976) 445.
[4] K. Naka, Y. Chujo, Chem. Mater. 13 (2001) 3245.
[5] W. Murphy, D.J. Mooney, J. Am. Chem. Soc. 124 (2002) 1990.
[6] B. Pokroy, E. Zolotoyabko, N. Adir, Biomacromolecules 7 (2006) 550.
[7] C.M. Zaremba, A.M. Belcher, M. Fritz, Y. Li, S. Mann, P.K. Hansma, D.E. Morse, J.S. Speck, G.D. Stucky, Chem. Mater. 8 (1996) 679.
[8] S. Weiner, L. Addadi, J. Mater. Chem. 7 (1997) 689.
[9] A. Sugawara, T. Kato, Chem. Commun. (2000) 487.
[10] A.W. Xu, M. Antonietti, H. Gölfen, Y.P. Fang, Adv. Funct. Mater. 16 (2006) 903.
[11] T. Hirai, S. Hariguchi, I. Komassawa, Langmuir 13 (1997) 6650.
[12] N. Gehrke, H. Gölfen, N. Pinna, M. Antonietti, N. Nassif, Cryst. Growth Des. 5 (2005) 1317.
[13] M. Lei, W.H. Tang, J.G. Yu, Mater. Res. Bull. 40 (2005) 656.
[14] S. Paria, K.C. Khilar, Adv. Colloid Interf. Sci. 110 (2004) 75.
[15] N. Hosoda, A. Sugawara, T. Kato, Macromolecules 36 (2003) 6449.
[16] S. Zhang, K.E. Gonsalves, Langmuir 14 (1998) 676.
[17] Q. Shen, Y. Chen, H. Wei, Y. Zhao, D. Wang, D. Xu, Cryst. Growth Des. 5 (2005) 1387.
[18] Y. Guo, L. Yang, X. Yang, X. Zhang, S. Zhu, K. Jiang, Macromol. Biosci. 3 (2003) 163.
[19] A. Sugawara, T. Ishii, T. Kato, Angew. Chem. Int. Ed. 42 (2003) 5299.
[20] J.P. Canselier, J. Dispers. Sci. Technol. 14 (1993) 625.
[21] D. Stitic, N. Filipovic-Vincekovic, H. Füredi-Milhofer, J. Crystal Growth 114 (1991) 118.
[22] D. Stitic, N. Filipovic-Vincekovic, R. Babiç-Ivancic, L. Tusek-Bozic, J. Crystal Growth 133 (1993) 189.
[23] M.J.J.M. Van Kemenade, P.L. De Bruyn, Colloids Surf. A 36 (1989) 359.
[24] H. Füredi-Milhofer, A. Kamyshyn, N. Garti, J. Crystal Growth 198/199 (1999) 1365.
[25] J. Yano, H. Furedi- Milhofer, E. Wachtel, N. Garti, Langmuir 16 (2000) 9996.
[26] J. Yu, M. Lei, B. Cheng, X. Zhao, J. Crystal Growth 261 (2004) 566.
[27] X. Zhang, Z. Zhang, Y. Yan, J. Crystal Growth 274 (2005) 550.
[28] H.M. Rietveld, Acta Crystallogr. 22 (1967) 151.
[29] R.A. Young, The Rietveld Method, IUCr, Oxford University Press, Oxford, UK, 1993.
[30] Program MAUD. Available from: 〈http://www.ing.unitn.it/~luttero/maud〉.
[31] M. Takiguchi, K. Igarashi, M. Azuma, H. Ooshima, Cryst. Growth and Des. 6 (12) (2006) 2754.
[32] S.R. Kamhi, Acta Crystallogr. 16 (1963) 770.
[33] B. Pokroy, J.S. Fieramosca, R.B. Von Dreele, A.N. Fitch, E.N. Caspi, E. Zolotoyabko, Chem. Mater. 19 (2007) 3244.
[34] Y. Pan, X. Zhao, Y. Sheng, C. Wang, Y. Deng, X. Ma, Y. Liu, Z. Wang, Colloids Surf. A: Physicochem. Eng. Aspects 297 (2007) 198.
[35] A. Schwartz, D. Eckart, J.O. Connel, K. Francis, Mater. Res. Bull. 6 (1971) 1341.
[36] Y. Ota, S. Inui, T. Iwashita, T. Kusaga, Y. Abe, J. Am. Ceram. Soc. 78 (1995) 1983.
[37] Y. Pan, X. Zhao, Y. Guo, X. Lv, S. Ren, M. Yuan, Z. Wang, Mater. Lett. 61 (2007) 2810.